American Mineralogist, Volume 92, pages 1474–1485 2007

Hydrogen bonded silanols in the 10 Å phase: Evidence from NMR spectroscopy

BRIAN L. PHILLIPS,[1,*] HARRIS E. MASON,[1] AND STEPHEN GUGGENHEIM[2]

[1]Department of Geosciences, Stony Brook University, Stony Brook, New York 11794-2100, U.S.A.
[2]Department of Earth and Environmental Sciences, University of Illinois at Chicago, Chicago, Illinois 60680, U.S.A.

ABSTRACT

Using ^{29}Si, ^{1}H, and ^{2}H magic-angle spinning (MAS) and ^{29}Si{^{1}H} heteronuclear correlation (HetCor) nuclear magnetic resonance (NMR) spectroscopy the tetrahedral sheets of the 10 Å phase are shown to contain Q^2-type Si bonded to silanol groups that donate hydrogen bonds to interlayer H_2O. ^{29}Si NMR spectra of 10 Å phase samples synthesized from oxide and from crystalline talc starting materials contain a peak near –87 ppm for Q^2 Si, in addition to the main peak at –98 ppm for the talc-like Q^3 of the tetrahedral sheet. The ^{1}H MAS NMR spectra of the 10 Å phase contain two distinct peaks, at chemical shifts of +7.8 and +3.2 ppm, in addition to a narrow peak near +0.9 ppm from the talc-like hydroxyl groups. ^{29}Si{^{1}H} HetCor data indicate that the +7.8 ppm ^{1}H resonance corresponds to silanol groups and that at +3.2 ppm arises from interlayer H_2O. Comparison of the observed data with correlations of ^{1}H NMR chemical shift and ^{2}H quadrupolar coupling indicates that the silanol groups donate moderate hydrogen bonds to interlayer H_2O, d(O···O) ≈ 2.8 Å, whereas most interlayer H_2O donate only very weak or no hydrogen bonds at ambient conditions. Our results suggest that formation of the 10 Å phase involves formation of vacancies, which allow favorable hydrogen bond interaction between interlayer H_2O and the normally hydrophobic talc-like 2:1 layers.

Keywords: NMR, 10 Å phase, talc, silanol, hydrogen bond

INTRODUCTION

The "10 Å phase" is a high-pressure product of talc and H_2O (Yamamoto and Akimoto 1977; Bauer and Sclar 1981). The name is derived from the d_{001} basal repeat, which is larger than that of talc (d_{001} = 9.5 Å) to accommodate H_2O in the interlayer, and reflects the fact that this phase has not been given a mineral name because it has not been reported from a natural assemblage. However, recent reports of a phyllosilicate with talc-like composition and ca. 10 Å layer repeat as inclusions in mantle olivine (Koch-Müller et al. 2006; Khisina and Wirth 2002), and observations of similar materials in products of experimental studies of antigorite dehydration (Perrillat et al. 2005) and equilibration of synthetic hydrous peridotite at elevated P and T (Fumagalli and Poli 2005) suggest that the 10 Å phase could form in nature through several different processes. Interest in the 10 Å phase derives from the possibility that this or similar materials could serve as a vehicle to carry H_2O into the mantle with subducting slabs. Several studies have reported on the chemistry and pressure/temperature stability of the 10 Å phase (Miller et al. 1991; Wunder and Schreyer 1992; Pawley and Wood 1995; Chinnery et al. 1999; Fumagalli et al. 2001), but the relationship between the interlayer H_2O and the 2:1 Mg-silicate layers, especially at pressure, is still not fully understood. Based on single-crystal X-ray diffraction (XRD) data, Comodi et al. (2005) presented the first crystal-structure analysis of the 10 Å phase, which shows a mica-like stacking with oxygen atoms of the H_2O molecules occupying the center of the 12-fold sites formed by two 6-membered silicate rings.

Until recently the 10 Å phase was thought to be a simple product of talc and H_2O in that the reaction product consisted of H_2O in an expanded interlayer between the 2:1 layers. However, Welch et al. (2006) report ^{29}Si NMR spectroscopic data and single-crystal electron microprobe results showing the 10 Å phase contains nearly 5% Si vacancies in the tetrahedral sheets. NMR spectra for samples prepared from both hydroxide/oxide mixtures and crystalline talc starting materials show a significant fraction of Q^2 Si. [Standard $Q^m(n\text{Al})$ notation to characterize the local environment of tetrahedrally coordinated Si is used throughout, where m is the number of bridging bonds to other tetrahedrally coordinated cations, and n is the number of adjacent Al4, where $0 \le n \le m$. For phases such as talc, which do not contain significant Al4, Q^m is used.] Welch et al. provide compelling data suggesting that these Q^2 sites are not associated with the edges of the particles. The Q^2 sites are not present in the crystalline talc starting material, indicating that they are created during the talc → 10 Å phase reaction. The ^{29}Si NMR results are supported by chemical analyses of single crystals synthesized from oxides that yield a Si/Mg ratio significantly lower than the 4:3 value expected for stoichiometric talc. Thus, the Q^2 sites probably occur adjacent to Si vacancies in the tetrahedral sheets. Although the implied vacancy concentration appears low (ca. 5%), each vacancy has up to three adjacent Q^2 Si. The termination of the broken Si-O-Si linkages at the vacancy will affect the interaction of H_2O with the tetrahedral sheet, the structure of the interlayer H_2O, and the interpretation of spectroscopic data that are needed to determine this structure.

* E-mail: brian.phillips@sunysb.edu

0003-004X/07/0809–1474$05.00/DOI: 10.2138/am.2007.2417

Here, we report the results of an NMR spectroscopic study for several samples of the 10 Å phase and its dehydration product. These data provide additional support for the conclusions of Welch et al. (2006) regarding the importance of vacancies in the structure of the 10 Å phase and allow assignments for the observed hydrogen species. Using two-dimensional NMR methods that correlate peaks from Si and H in close spatial proximity, we show that the Q^2 are terminated by silanol groups that serve as moderate hydrogen bond donors to interlayer H_2O molecules.

Experimental methods

Sample materials

Several samples of the 10 Å phase were studied, with the most comprehensive set of data obtained for a sample from the same batch used by Miller et al. (1991) and denoted "S01." This sample was synthesized at 450 °C and 5 GPa from a mixture of MgO, SiO_2, and H_2O, following the methods of Sclar et al. (1987). Based on partial Rietveld refinement, the sample comprises approximately 80% by wt% 10 Å phase, 11 wt% coesite, and 9 wt% brucite (Bish and Guggenheim, unpublished data). Bauer and Sclar (1981) reported that the particle size for material produced under similar conditions is about 5 µm. Miller et al. (1991) noted that Debye-Scherrer X-ray powder patterns showed broad lines indicating either particle size variations or poor crystallinity. For comparison, a talc sample (S01d) was prepared by dehydrating a 50 mg portion of 10 Å phase S01 by heating at 525 °C for 40 min in a preheated furnace in an open Pt crucible. This temperature is well within the stability field of talc (Miller et al. 1991) and below that for the decomposition of brucite (782 °C; Johnson and Walker 1993). X-ray powder diffractograms (Siemens D-5000 diffractometer, Cu radiation, graphite monochromator, 40 kV, 20 mA, 2θ range of 2–40° at steps of 0.02° and count time of 0.5 s) taken both before and after heating indicated complete transformation of the 10 Å phase to talc.

Partially deuterated 10 Å phase samples were produced from isotopically normal talc + D_2O at 6.5 GPa, 650 °C (24 h), with single-run samples denoted HM-0303 and HM-0305. The talc (25–26 mg) and D_2O (8 µL) were loaded into a silver capsule 4 mm long and 3.5 mm outside diameter sealed by a press-fit cap. Pressure was applied by a 1000 ton Kennedy-Walker type uniaxial split cylinder multi-anvil press (USCA-1000). The initial ^{1}H-NMR and XRD data for runs HM-0303 and HM-0305 were identical and showed that complete conversion to 10 Å phase had occurred. These samples were then combined (denoted HM-03) for subsequent ^{2}H and ^{1}H NMR analysis. ^{29}Si NMR data for a similarly prepared sample that was partially transformed to a mixture of talc and 10 Å phase were reported by Welch et al. (2006).

NMR spectroscopy

The NMR spectra were recorded with a 400 MHz (9.4 T) Varian Inova spectrometer at frequencies of 79.5 MHz for ^{29}Si and 399.98 MHz for ^{1}H. The ^{29}Si-observe NMR experiments used Varian/Chemagnetics T3-type probe assemblies configured for 7.5 and 3.2 mm rotors. For the ^{1}H single-pulse (SP) MAS experiments a 4 mm Chemagnetics MAS probe was used, which had been modified to yield very low ^{1}H-background. The ^{1}H MAS NMR background signal in this configuration is about three decades smaller than that from the samples and was not removed from the spectra.

The ^{29}Si{^{1}H} cross-polarization MAS (CP/MAS) spectra were obtained at spinning rates of from 3–5 kHz and contact times that varied from 0.2 to 20 ms. CP kinetics curves were measured on-resonance at a spinning rate of 3 kHz with continuous wave (CW) irradiation at the $n = -1$ sideband match condition. For other CP/MAS spectra the transverse ^{29}Si field (γB_1) was ramped over approximately 6 kHz, centered near the first sideband match. Quantitative ^{29}Si SP/MAS data were obtained only for sample S01, using 5 µs pulses (90°), a 5 kHz spinning rate, and relaxation delays of 300–3600 s. Proton decoupling was employed during acquisition of all ^{29}Si SP and ^{29}Si{^{1}H} CP/MAS spectra, but the spectra show no significant dependence on the strength of the decoupling field.

The 2-dimensional (2-d) ^{29}Si{^{1}H} heteronuclear correlation (HetCor) spectra were measured at a spinning rate of 10.4 kHz with an increment of 20 µs in $t1$, corresponding to an $F1$ frequency window of 50 kHz. The 2-d data correspond to 128 hypercomplex points in $t1$, each corresponding to 320–880 acquisitions. Standard forward linear prediction methods were used to complete the signal from the narrow hydroxyl ^{1}H resonance and avoid truncation artifacts. The experimental parameters for the amplitude-ramped CP were optimized on the sample for best signal-to-noise ratio.

The ^{2}H-MAS/NMR spectra were acquired at 91.1 MHz (14.1 T) on a Bruker Avance 600 spectrometer using a 4 mm Bruker probe assembly and spinning rate of 12.5 kHz. Quadrupolar coupling parameters were obtained by a least-squares fit of the integrated spinning sideband (SSB) intensities using the STARS simulation package (Varian, Inc.). We report the chemical shifts for both ^{29}Si ($\delta_{Si\text{-}29}$) and ^{1}H ($\delta_{H\text{-}1}$) relative to tetramethylsilane (TMS). For ^{29}Si an external sample of kaolinite was used as a solid-state reference, which gives peaks at $\delta_{Si\text{-}29} = -90.86(2)$ and –91.50(2) ppm. Reagent-grade hydroxylapatite was used as a secondary ^{1}H standard, with the chemical shift of its hydroxyl resonance taken to be $\delta_{H\text{-}1} = +0.2$ ppm (Yesinowski and Eckert 1987).

Results

^{29}Si SP and ^{29}Si{^{1}H} CP/MAS NMR

The 10 Å phase sample S01 gives ^{29}Si SP and CP/MAS NMR spectra that contain a peak at a chemical shift of $\delta_{Si\text{-}29} = -98$ ppm for talc-like Q^3 sites, and a second main peak at –87 ppm assigned to Q^2 Si configurations (Figs. 1a and 1b). These spectra closely resemble those presented by Welch et al. (2006) for 10 Å phase samples prepared at higher P (6.5 vs. 5 GPa) and T (650 vs. 450 °C). The sharp peaks at $\delta_{Si\text{-}29} = -106$ and –112 ppm in the SP spectrum (Fig. 1a) arise from coesite impurity that was also noted in the XRD patterns. The Q^3 peak at –97.9(1) ppm occurs near the chemical shift reported for talc, –97.8 ppm. (Mägi et al. 1984), but exhibits a pronounced asymmetry that can be fit by a second unresolved peak near –97 ppm. The HetCor data presented below show that these Q^3 environments at –97 ppm are closest to the interlayer H_2O. Additional poorly resolved intensity occurs in the

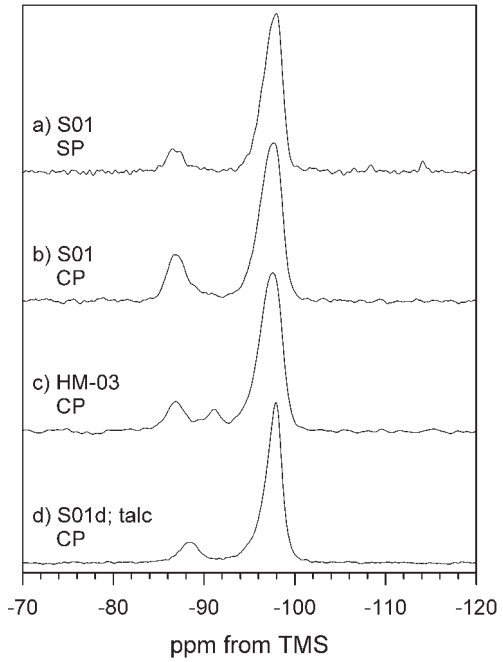

Figure 1. ^{29}Si MAS NMR spectra of the 10 Å phase samples and talc dehydration product. (**a**) S01 10 Å phase, obtained with single-pulse excitation and 2400 s relaxation delay; (**b**) S01 10 Å phase, CP/MAS with 7 ms contact time; (**c**) HM-03 10 Å phase, CP/MAS, 10 ms contact time; (**d**) S01d talc, CP/MAS, 7 ms contact time. All spectra obtained at a spinning rate of 5.0 kHz.

range –88 to –91 ppm that is clearly seen in the CP/MAS spectra (Fig. 1b) and which includes an apparent shoulder near –89 ppm, indicating some distribution of Q^2 environments.

Welch et al. (2006) interpret the Q^2 signal as arising from sites adjacent to Si vacancies in the tetrahedral sheet; all of the results of the present study support this interpretation. Assignment of the peak near $\delta_{Si\text{-}29}$ = –87 ppm to Q^2 configurations is consistent with the separations of 5 to 10 ppm between Q^2 and Q^3 found for other alkaline earth silicates (Mägi et al. 1984; Rocha et al. 1991). Although the chemical shift ranges of both Q^2 and Q^3(0Al) environments overlap the –86 to –89 ppm range, all Q^3(0Al) in trioctahedral phyllosilicates fall outside this range (Weiss et al. 1987). Peaks near –84 ppm occur in spectra of Al-poor sepiolite and palygorskite and were also assigned to Q^2(0Al) configurations (Barron and Frost 1985; Espinose de la Caillerie and Fripiat 1994).

For ^{29}Si SP spectra taken under quantitative conditions (3600 s relaxation delay) the integrated intensity of the Q^2 peak represents 9.9% of the signal from the S01 10 Å phase, excluding the coesite peaks. This Q^2 fraction is significantly smaller than that reported by Welch et al. (2006) for a sample also prepared by oxides/hydroxides, but at higher *P* and *T*. For this sample, we noted substantially different relaxation times for the two peaks, such that the Q^2 peak is enhanced at shorter relaxation delays (e.g., 16.6% at 300 s).

Sample HM-03, synthesized from talc + water, gives ^{29}Si CP/MAS spectra with similar peaks at –98 and –87 ppm, but which also contain a peak at –91 ppm (Fig. 1c). This peak appears to be enhanced relative to the peaks at –87 and –98 ppm in CP/MAS spectra at short contact times (1 ms). Assignment of the –91 ppm peak is uncertain, but its chemical shift and CP enhancement are similar to Q^2 sites of silica gels, which are bonded to two silanol groups. Unfortunately, limited sample size prevents more detailed analysis or measurement of a quantitative ^{29}Si SP spectrum. Comparison of CP/MAS spectra of this sample with those of sample S01 taken under identical conditions (1 and 10 ms contact time, 5 kHz spinning rate, ramped CP) suggests that the combined peaks at –87 and –91 ppm represent about 11–12% of the intensity, slightly higher than for the Q^2 in sample S01.

For comparison, we have also obtained NMR data for a portion of S01 that was dehydrated to talc (denoted S01d). The ^{29}Si CP/MAS spectra (Fig. 1d) are similar to those of the 10 Å phase parent, except that the Q^2 peak is shifted to –88 ppm and the Q^3 peak is more narrow and symmetrical. Although limited sample size prevented us from obtaining fully relaxed SP spectra, the integrated peak ratios were similar to those for the 10 Å phase parent taken under the same conditions. These data indicate that the Q^2 sites in the 10 Å phase remain after removal of interlayer H_2O.

The variation of ^{29}Si{^{1}H}CP/MAS intensity for both S01 (10 Å phase) and S01d (talc) show significant differences between the Q^2 and Q^3 peaks (Fig. 2). For both samples, the Q^2 intensity is enhanced at short contact times consistent with stronger Si-H dipolar coupling, which can be interpreted as a larger number of nearby H or shorter Si-H distances, or both. For S01, the Q^2 exhibit a classical CP build-up curve characterized by a cross-relaxation time of $T_{Si\text{-}H}$ = 1.2 ms and a very long $T_{1\rho,H}$ (> 100 ms). This $T_{Si\text{-}H}$ value lies in the range of those reported by Oglesby and Stebbins (2000) for Si sites in minerals known to contain silanol groups (0.6 to 1.2 ms). In contrast, the increase of CP intensity for the Q^3 peak is slower and more similar to that shown by Oglesby and Stebbins (2000) for talc, which they fit to a classical CP kinetics curve with $T_{Si\text{-}H}$ = 3.6 ms. In a rigid system, the CP build-up rate ($T_{Si\text{-}H}^{-1}$) is proportional to a sum over the Si-H distances as $T_{Si\text{-}H}^{-1} \propto \Sigma d(Si\text{-}H)^{-6}$, and thus very sensitive to the distance from Si to the nearest protons. The build-up of Q^3 CP/MAS intensity of the 10 Å phase is more complicated than that for the Q^2 sites and cannot be fit by classical exponential CP kinetics (Kolodziejski and Klinowski 2002). This behavior could

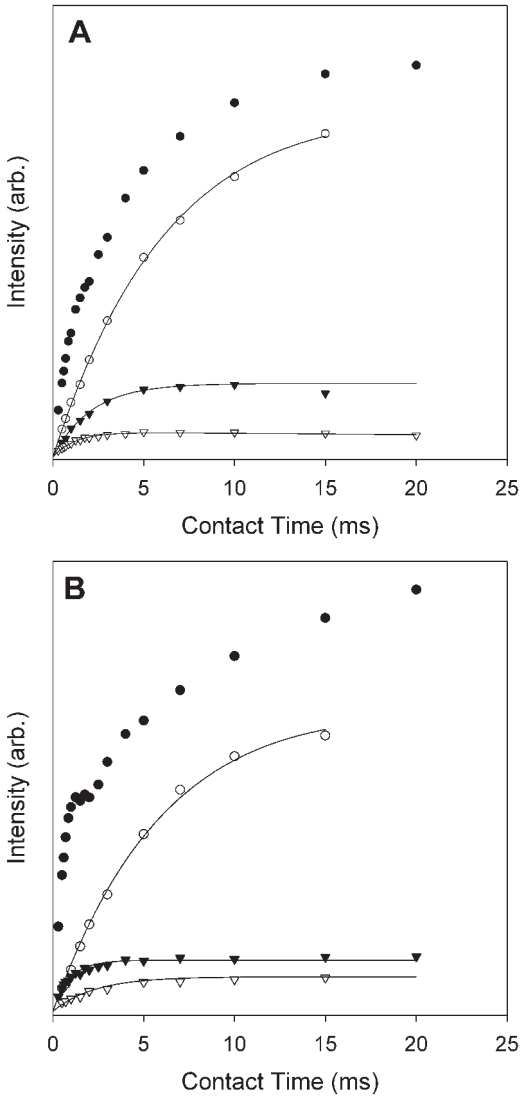

FIGURE 2. Variation of ^{29}Si{^{1}H} CP/MAS intensity with contact time for (**a**) S01 10 Å phase, and (**b**) S01d talc. Symbols represent intensity integrated over the Q^2 (triangle) and Q^3 (circle) lineshapes. Data acquired at 3.0 kHz spinning rate at the $n = -1$ sideband match condition with no modulation of the RF fields (closed symbols); and at 10.4 kHz with ramped CP (open symbols), the conditions used for HetCor. Lines represent least-squares fits to classical CP dynamics.

arise in part from the presence of a sub-set of Q^3 more strongly coupled to interlayer H_2O. However, we have also observed complex CP behavior for pure talc under these experimental conditions. In this case, the CP build-up curve exhibits oscillations owing to the very weak homonuclear ^1H-^1H coupling in talc, which is effectively averaged even with the slow spinning rate used for these experiments (3 kHz). Similar oscillations are apparent in the data presented by Oglesby and Stebbins (2000). Modulation of the transverse B_1 fields during the polarization transfer removes the oscillations in the CP dynamics (e.g., Fig. 2, open symbols), but the resulting apparent $T_{Si\text{-}H}$ values depend on the experimental conditions.

For the S01d (talc), the Q^2 sites also show classical CP behavior with a $T_{Si\text{-}H}$ value of 0.9 ms, which is somewhat shorter than observed for the parent 10 Å phase. This decrease of cross-relaxation time with removal of interlayer H_2O could reflect reduced rotational motion of the silanol groups with collapse of the interlayer spacing. In contrast, the Q^3 intensity shows a much slower increase of CP intensity with contact time compared with 10 Å phase, and more pronounced oscillations, indicating that the CP behavior of the Q^3 is much more affected by removal of the interlayer H_2O.

^{1}H MAS NMR

The ^{1}H MAS NMR spectrum of each 10 Å phase sample (Fig. 3) contains three main resonances with chemical shifts near $\delta_{H\text{-}1}$ = 1, 3.5, and 7.8 ppm. However, there are differences in peak positions and intensities among the samples, and for a single sample with storage time (HM-0305 vs. HM-03) that indicate significant variability in the H environments. The ^{1}H MAS NMR spectra of S01 contain three main resonances with chemical shifts of $\delta_{H\text{-}1}$ = 0.9, 3.2, and 7.8 ppm (Fig. 3a). These resonances are most clearly discerned in the spinning sidebands (SSBs; Fig. 3, inset), because the peak at 3.2 ppm is relatively broad (3.5 ppm full-width at half-maximum; FWHM) and concealed by several narrow but minor peaks in the range 4.8 to 2.4 ppm. The pronounced spinning sidebands (Fig. 3, inset) observed for the peaks at 3.2 and 7.8 ppm indicate strong homonuclear ^{1}H-^{1}H coupling for these H. The chemical shift of the narrow peak at 0.9 ppm is very similar to that of talc (Yesinowski et al. 1988) and is assigned to the talc-like hydroxyl groups (Mg_3-OH) of the 2:1 layers. Talc-like regions give narrow ^{1}H peaks and small spinning sidebands for MAS NMR because of the weak coupling to other protons (large H-H distances, low H density). The narrow peak at 4.5 ppm is probably related to surface-sorbed H_2O and that at 2.4 ppm is of unknown origin and was not observed for other 10 Å phase samples or in the HetCor spectra; these signals were omitted from further analysis. At these experimental conditions, the brucite impurity as detected by XRD should contribute a very broad signal under the center band and give significant SSBs, owing to the very strong ^{1}H-^{1}H coupling.

The ^{1}H spectral parameters for all samples (Table 1) were obtained by fitting the center band and the first two pairs of SSBs to a sum of curves with mixed Lorentzian/Gaussian shape. To obtain physically relevant fits for sample S01, we constrained the width and position for the center band component at 3.2 ppm to equal the average of the best-fit values obtained for the $n = \pm 1$ SSBs of this resonance, because it is not resolved in the center band. In addition, we added a broad component to the center band and the SSBs to account for the brucite impurity. The width and positions of the peaks representing the brucite component were constrained to equal those obtained by fitting the broad resonance apparent in the spectra of the dehydrated sample (S01d talc; Fig. 3f), which probably also arises from brucite impurity (vide infra). The resulting H distribution (Table 1) remains somewhat uncertain, because of these assumptions and the difficulty of modeling ^{1}H MAS peak shapes owing to the combination of homonuclear ^{1}H-^{1}H coupling and a chemical shift anisotropy of comparable magnitude. Nonetheless, because the peaks at

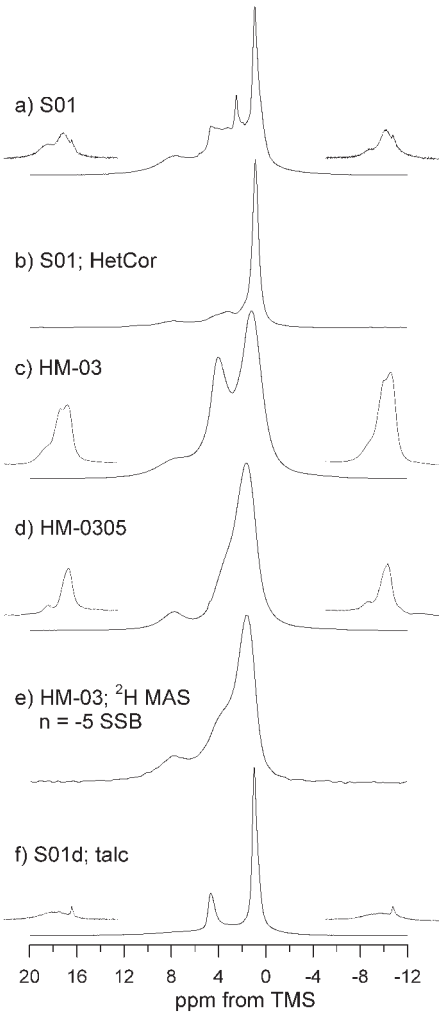

FIGURE 3. ^{1}H and ^{2}H MAS/NMR spectra of 10 Å phase and talc samples. (**a**) ^{1}H MAS, S01 10 Å phase; (**b**) ^{29}Si-detected ^{1}H MAS of S01 10 Å phase, obtained as the summed HetCor projection (–85 to –102 ppm) at 15 ms contact time (ν_{rot} = 10.4 kHz). (**c**) ^{1}H MAS, HM-03 10 Å phase, 4 months after synthesis; (**d**) ^{1}H MAS, HM-0305 10 Å phase, 2 days after synthesis; (**e**) ^{2}H MAS, HM-03 10 Å phase, n = –5 spinning sideband shifted by $-n\cdot\nu_{rot}$, ν_{rot} = 12.5 kHz. (**f**) ^{1}H MAS,S01d talc dehydration product from 10 Å phase. Insets show the $n = \pm 1$ spinning sidebands for ^{1}H MAS spectra at 5× vertical scaling and shifted relative to each other by the spinning rate, ν_{rot} = 15–16 kHz.

TABLE 1. ^{1}H and ^{2}H MAS NMR results for the samples studied

Sample (experiment)	δ_H (ppm)	Relative intensity (±0.02)		FWHM (ppm)	C_q (kHz)	η	Assignment
		total	10 Å				
S01 (^{1}H-MAS)	0.9	0.29	0.43	1.1			Mg_3-OH
	2.4	0.05		0.6			imp(?)
	3.2	0.30	0.45	3.2			interlayer H_2O
	4.5	0.03		0.5			surface water
	7.8	0.08	0.12	3.0			silanol (+H_2O?)
	5	0.25		10			(brucite imp.)
S01 (HetCor)*	0.9	0.63		0.8			Mg_3-OH
	3.3	0.26		3.4			interlayer H_2O
	7.9	0.11		3.4			silanol
HM-03 (^{1}H MAS)	1.2	0.49		3.7			Mg_3-OH
	3.7	0.40		1.8			interlayer H_2O
	7.6	0.11		2.1			silanol
HM-03 (^{2}H MAS)	1.7	0.48			300(10)	≈0	Mg_3-OH
	3.5	0.40			n.d.†	n.d.	interlayer H_2O
	7.7	0.12			210(10)	0.1(1)	silanol
	4.8						surface water
HM-0305 (^{1}H MAS)	1.6	0.52		1.7			Mg_3-OH
	3.3	0.39		2.6 (3.5‡)			interlayer H_2O
	7.8	0.09		2.3			silanol
S01d talc (^{1}H MAS)	0.9	0.50		0.7			Mg_3-OH
	3.8	0.10		2.2			silanol
	4.6	0.09		0.6			surface water
	5	0.31		10			(brucite)

Note: HetCor results are for the *F*1 projection summed from $\delta_{Si\text{-}29}$ = –86 to –100 ppm.
* Summed projection, 15 ms contact time.
† Not determined.
‡ For spinning sidebands.

0.9 ppm (29%) and 7.8 ppm (8%) are relatively well resolved in the center band and SSBs, these fitted relative intensities are probably a reasonable representation of the H distribution in this sample. The resulting intensities are given in Table 1, and those for the peaks at 0.9, 3.2, and 7.8 ppm are re-normalized with the assumption that these peaks correspond to the 10 Å phase. The fraction of the ^{1}H NMR signal intensity attributed to brucite agrees well with the ca. 9 wt% estimated from the XRD data. This assemblage corresponds to a ratio of hydroxyl groups in 10 Å phase:brucite of 1.3:1, compared to 1.2:1 for the intensity ratio at 0.9 ppm to the fitted broad component.

A similar set of three resonances occurs in ^{1}H MAS spectra of the partially deuterated samples HM-03 and HM-0305 (Figs. 3c and 3d), but with intensity ratios that differ somewhat from those for sample S01 (Table 1). In particular, the relative intensity for the main hydroxyl peak is higher, suggesting lower total H_2O content for these samples compared to S01. We observed significant differences in the ^{1}H NMR spectra taken shortly after synthesis (HM-0305; Fig. 3d) and four months later (HM-03; cf. Fig. 3c). With storage, the peak near 3.5 ppm shifted from 3.3 to 3.7 ppm and narrowed significantly, from 2.6 to 1.8 ppm FWHM, although a broader component remains that is evident in the SSBs. In addition, the main hydroxyl peak shifted from 1.6 to 1.2 ppm, but remained at a chemical shift higher than that observed for sample S01 (0.9 ppm). These differences are unlikely to be related to H/D exchange with atmospheric H_2O, because the relative intensities did not vary significantly and we expect water molecules to be more labile to H/D exchange than hydroxyl groups. For both HM-03 and HM-0305, the peak near 3.5 ppm exhibits a set of SSBs that span approximately 80 kHz, which suggests that it contains a contribution from rigid H_2O molecules (Yesinowski et al. 1988). For the deuterated samples, some of the lineshape differences between the center band and SSBs could arise from local environments composed of different isotopomers.

The ^{1}H MAS/NMR spectrum of the S01d talc derived from dehydrating the S01 10 Å phase appears to contain only relatively narrow peaks at $\delta_{H\text{-}1}$ = 0.8 ppm for Mg_3-OH groups and 4.6 ppm for surface-adsorbed H_2O. The SSBs indicate the presence also of a very broad signal (10 ppm FWHM) that likely arises from the brucite impurity. The fitted spectral analysis for this sample (Table 1) includes a fourth peak at $\delta_{H\text{-}1}$ = 3.8 ppm (2.2 ppm FWHM) that corresponds to a signal observed in the $^{29}Si\{^{1}H\}$ HetCor spectra described below, but which is not resolved in this SP/MAS spectrum. The relative intensity for this peak was estimated by constraining its position and width to equal those in the HetCor spectra (described below) and allowing all other parameters to vary. The resulting fit is significantly improved relative to those obtained using three components. The peak at 3.8 ppm fills the intensity apparent between the peaks at 4.6 and 0.9 ppm (Fig. 3f). Assignment of the main ^{1}H NMR peaks for these samples is discussed below.

^{2}H MAS NMR

The ^{2}H MAS/NMR spectrum for the partially deuterated sample HM-03 (Fig. 4) contains three sets of spinning sidebands with chemical shifts of $\delta_{H\text{-}2}$ = 1.7, 3.5, and 7.7 ppm that closely resemble the ^{1}H NMR peaks of this same sample (Table 1), plus a large, poorly resolved center band. The isotropic chemical shifts were obtained as the average positions of the SSB pairs

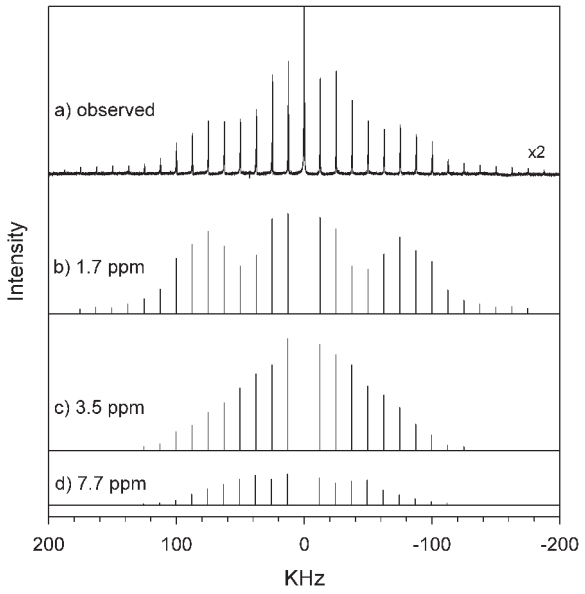

FIGURE 4. (**a**) ^{2}H MAS/NMR spectrum of HM-03 10 Å phase; (**b–d**) spinning sideband envelopes for three components centered at chemical shifts of (**b**) 1.7 ppm, (**c**) 3.5 ppm, and (**d**) 7.7 ppm. Spinning sidebands in **b–d** are plotted as lines with height proportional to the integrated intensity of the corresponding peak obtained by fitting each SSB in **a** to a sum of three (or two) curves (see Fig. 3e). Spectrum acquired at 91.1 MHz and a spinning rate of 12.500 kHz.

from $n = \pm3$ to $n = \pm7$. The ^{2}H SSB at $n = -5$ is plotted with the ^{1}H MAS NMR spectra (Fig. 3e), offset by five times the spinning frequency for direct comparison with the ^{1}H MAS spectra. The center band is dominated by a peak at 4.8 ppm that probably contains a significant contribution from surface adsorbed $(H,D)_2O$, but could also represent interlayer water molecules undergoing rapid isotropic reorientation. Although this peak dominates the center band, it does not give a distinct peak in the spinning sidebands and as a result represents <15% of the total intensity. In addition, no corresponding narrow signal was observed in the ^{1}H spectra of this sample (Fig. 3), so the center band was not analyzed further.

The profiles of the three spinning sideband envelopes were obtained by fitting each of the SSBs to a sum of 2–3 pseudo-Voigt curves and plotting the resulting integrated intensities as a "stick diagram" (Figs. 4b–4d). The most intense resonance is near $\delta_{H-2} = +1.7$ ppm and gives a broad SSB envelope characterized by a quadrupolar coupling constant of $C_q = 300(10)$ kHz and asymmetry parameter $\eta \approx 0$, consistent with a rigid hydroxyl group. The second most intense SSB set ($\delta_{H-2} = 3.5$ ppm) has an intermediate profile that appears to contain a large contribution from water molecules undergoing 180° flips about the H-O-H bisector (Eckert et al. 1987). The third SSB envelope, at $\delta_{H-2} \approx$ 7.7 ppm, has a smaller width and can be fit with a $C_q = 210(10)$ kHz and small asymmetry parameter ($\eta \approx 0.1$). The similarity of the relative integrated intensities of these three powder patterns, 0.48:0.40:0.12, to those for the ^{1}H MAS spectra of this sample suggests that isotopic equilibrium between the D_2O and isotopically normal talc had been reached during the synthesis.

^{29}Si{^{1}H} HetCor

The ^{29}Si{^{1}H} HetCor experiment provides a direct correlation between the peaks observed in the ^{29}Si and ^{1}H NMR spectra. These data are obtained as ^{29}Si CP/MAS spectra ($F2$ dimension) that are modulated according to the chemical shifts for the ^{1}H nuclei ($F1$ dimension) from which magnetization is transferred during the CP contact time (Zumbulyadis 1986; Fyfe et al. 1992). In our experiments no ^{1}H-^{1}H decoupling was applied during $t1$, which allows ^{1}H signal in $F1$ to be observed for more distant ^{1}H nuclei at long contact times, via spin diffusion processes. No signal can occur for anhydrous phases or those lacking Si (e.g., coesite and brucite impurities). Sufficient sample was available for these 2-d experiments only for the 10 Å phase S01 and its talc dehydration product S01d.

A 2-d HetCor contour plot is shown in Figure 5 for sample S01, but the changes that occur with increasing contact time are more clearly displayed as cross-sections in $F1$ (^{1}H traces) taken at the Q^2 and Q^3 chemical shifts (Fig. 6). The contour plot, obtained at a relatively short contact time (2 ms), shows a strong cross peak between the Q^3 Si and the main ^{1}H peak at $\delta_{H-1} = 0.9$ ppm, plus much smaller cross peaks at $\delta_{H-1} = 3.1$ and 7.8 ppm. Note that the peak intensity for these smaller ^{1}H cross-peaks occurs at $\delta_{Si-29} = -97$ ppm, which is offset from the ^{29}Si peak maximum and in the direction of the asymmetry shown in the ^{29}Si SP and CP/MAS spectra. The Q^2 show cross-peaks at the same ^{1}H chemical shifts as for the Q^3, but those at $\delta_{H-1} = 7.8$ and 3.1 ppm are much more intense compared with that at 0.9 ppm. The summed ^{1}H projection shows peaks at nearly the same positions as the main peaks found for the ^{1}H MAS spectrum (cf. Fig. 3). The narrow ^{1}H MAS peaks at $\delta_{H-1} = 4.5$ and 2.4 ppm are missing from the HetCor spectrum, indicating that these H are not coupled to Si, either because of rapid motion, or because they occur in a separate phase. The observation of the same ^{1}H cross peaks for both the Q^2 and the Q^3 Si indicates that these Si are located near the same H environments, constituting strong evidence that the Q^2 sites occur in the 10 Å phase.

At short contact time (1–2 ms), about one-half the intensity in the ^{1}H trace at the Q^2 position occurs in the peak at $\delta_{H-1} = 8$ ppm (Fig. 6), with the peaks at 3.1 and 0.9 ppm increasing with increasing contact time. These changes probably arise from ^{1}H-^{1}H spin diffusion, because the total Q^2 intensity does not increase significantly beyond about 5 ms under these conditions (Fig. 2a, open symbols). The CP kinetics for both Q^2 and Q^3 signals displayed classical behavior with T_{Si-H} values of 1.2(1) and 5.7(2) ms, respectively, under the HetCor experimental conditions (ν_{rot} = 10.4 kHz, ramped CP; Fig. 2a). For the Q^3 sites, the cross peaks at 8 and 3.1 ppm increase with increasing contact time, as does the total Q^3 intensity. Comparison of traces at $\delta_{Si-29} = -97$ and –98 ppm (Fig. 6, top) shows that the Si environments with more positive chemical shifts are located closer to the H which give the peaks at $\delta_{H-1} = 8$ and 3.1 ppm. The ^{1}H traces also contain broad SSBs, which indicate a population of strongly coupled protons in H-rich portions of the sample that are not clearly resolved in the center band.

An alternate view that aids assignment of the ^{1}H peaks is provided by the $F2$ cross sections (^{29}Si traces) at the $F1$ positions of the main ^{1}H peaks (Fig. 7) as a function of contact time. The traces at $\delta_{H-1} = 8$ ppm (Fig. 7a) clearly show that the cor-

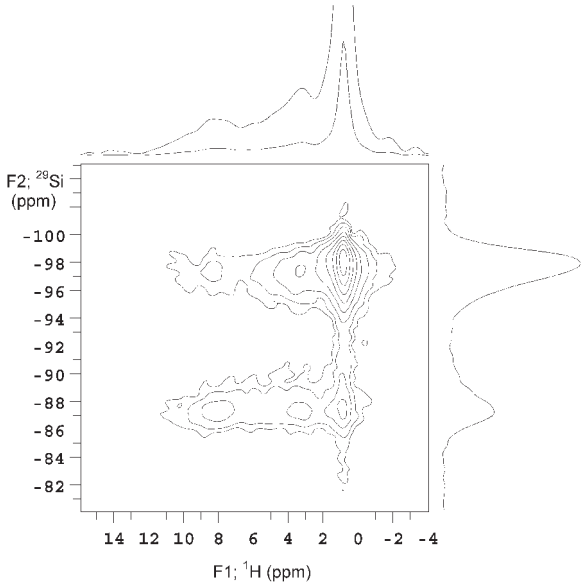

FIGURE 5. 2-d $^{29}Si\{^{1}H\}$ HetCor spectrum of S01 10 Å phase at contact time of 2 ms and ν_{rot} = 10.4 kHz. Spectra at top and side are summed projections; top trace is shown at 5× vertical scaling.

responding H are strongly coupled to the Q^2 sites, with most of the cross-peak intensity at short contact time occurring at $\delta_{Si\text{-}29}$ = –87. The Q^3 cross-peak intensity increases with longer contact time, indicating longer Si-H distances. The traces at $\delta_{H\text{-}1}$ = 3.1 ppm (Fig. 7b) show a more constant distribution of cross-peak intensity for Q^2 and Q^3, having a ratio of 0.36:0.64 at 1–2 ms, reflecting the Q^2:Q^3 ratio in the immediate vicinity of these H. A gradual increase of the Q^3 intensity beyond about 5 ms arises from longer-range interactions. The *F*2 cross sections at the main hydroxyl resonance ($\delta_{H\text{-}1}$ = 0.9 ppm, Fig. 7c) provide an interesting contrast, showing a relative Q^2:Q^3 intensity that does not vary significantly with contact time and is very similar to that observed in the ^{29}Si SP spectra (cf. Fig. 1a). Because the Mg_3-OH sites are distributed throughout the 10 Å phase and are equidistant from the Q^2 and Q^3, they sample the average Si distribution.

For comparison, we also obtained $^{29}Si\{^{1}H\}$ HetCor spectra for the S01d talc dehydration product of the 10 Å phase. The 2-d contour plots and projections (Fig. 8) show two distinct ^{1}H cross-peaks, one for the main Mg_3-OH groups at $\delta_{H\text{-}1}$ = 0.8 ppm, and a much smaller peak at 3.8 ppm. The summed ^{1}H projection (Fig. 8, top) differs significantly from the ^{1}H-MAS spectrum of this sample (cf. Fig. 3f), lacking the narrow peak near +4.6 ppm but showing the peak at 3.8 ppm. The ^{1}H cross-sections (*F*1) at the Q^2 peak position (Fig. 9) show sub-equal cross-peak intensity at $\delta_{H\text{-}1}$ = 3.8 and 0.8 ppm at short contact time (1.5–2 ms), with the 0.8 ppm peak increasing at longer contact times. The peak position and width observed for the 3.8 ppm cross-peak was used for the fitting the ^{1}H MAS spectra as described above (Table 1). The trace at the Q^3 position is dominated by the peak for Mg_3-OH but also contains a weak signal near +3.6 ppm that increases with contact time.

The ^{29}Si traces (Fig. 10) show that the ^{1}H peak at 3.8 ppm is strongly coupled to both Q^2 and Q^3 type Si, giving approximately

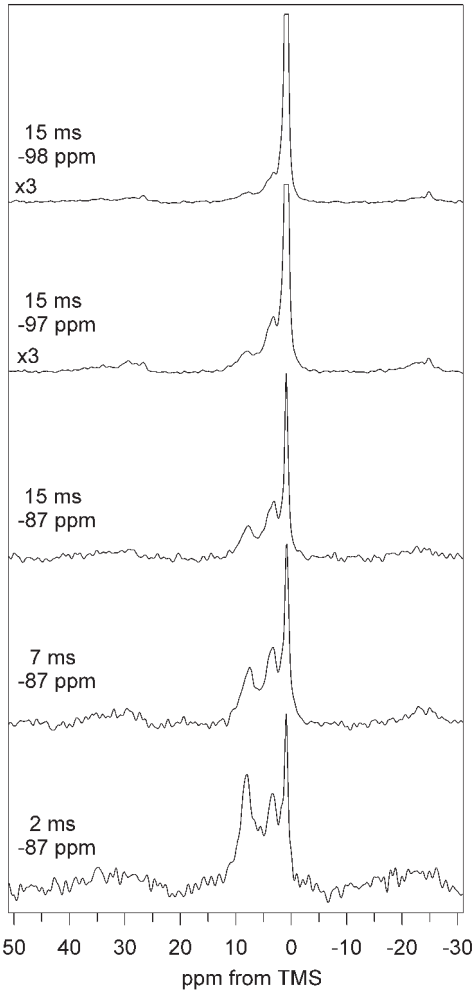

FIGURE 6. ^{1}H traces (*F*1) from $^{29}Si\{^{1}H\}$ HetCor spectra of S01 10 Å phase taken at the Q^2 peak position ($\delta_{Si\text{-}29}$ = –87 ppm) for the indicated contact times, and at a contact time of 15 ms for Q^3 positions at $\delta_{Si\text{-}29}$ = –97 ppm (peak at $\delta_{H\text{-}1}$ = 3.1 and 8 ppm) and at $\delta_{Si\text{-}29}$ = –98 ppm (peak at $\delta_{H\text{-}1}$ = 0.9 ppm).

equal intensities at short contact time (1–2 ms). At longer contact times (7–15 ms), the Q^3 peak continues to increase. This result reflects the CP dynamics under these conditions (Fig. 2b, open symbols), which show that the Q^2 intensity does not increase beyond 5 ms, but that the Q^3 intensity continues to increase with contact time. The *F*2 cross-sections at the Mg_3-OH peak are very similar to those observed for the S01 10 Å phase (cf. Figs. 10b and 7c) and show almost no change with contact time.

DISCUSSION

Assignment of ^{1}H NMR resonances and H distribution in the 10 Å phase

Although there are clearly some differences in detail among the samples studied, the distinctive H-environments in the 10 Å phase vs. talc appear to correspond primarily to the ^{1}H NMR peaks near $\delta_{H\text{-}1}$ = 7.8 and 3.2–3.6 ppm. The ^{1}H NMR chemical shift correlates strongly with hydrogen bond distance (e.g.,

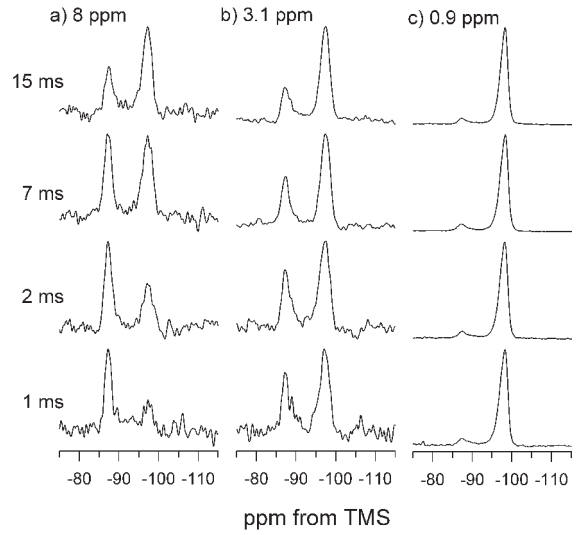

FIGURE 7. ^{29}Si traces ($F2$) from ^{29}Si{^{1}H} HetCor spectra of S01 10 Å phase taken at the indicated contact times, corresponding to cross-sections at the main ^{1}H peak positions in $F1$ at $\delta_{H\text{-}1}$ = 8 ppm (**a**), 3.1 ppm (**b**), and 0.9 ppm (**c**).

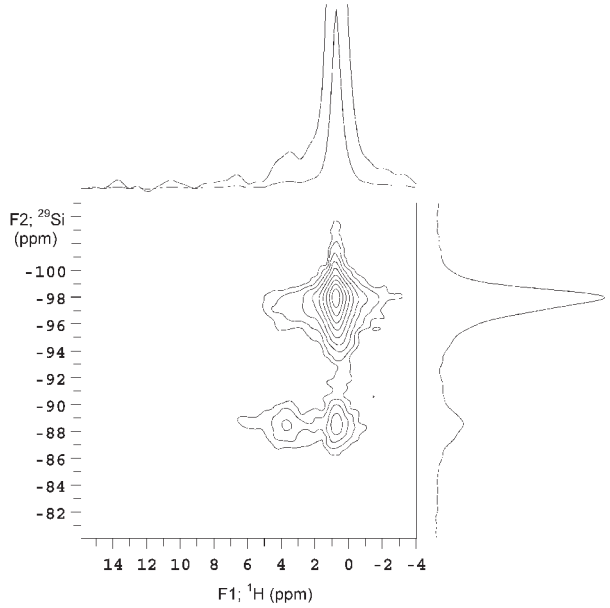

FIGURE 8. 2-d ^{29}Si{^{1}H} HetCor spectrum of S01d talc from dehydration of 10 Å phase, taken at a contact time of 2 ms and ν_{rot} = 10.4 kHz. Spectra at top and side are summed projections; top trace is shown at 5× vertical scaling.

Yesinowski et al. 1988) but less specifically with the oxygen environment (e.g., Mg-OH, H_2O, silanol). Thus, the peak at 7.8 ppm corresponds to the H participating in the strongest hydrogen bonds. Based on the strong coupling of these H to the Q^2 sites observed in the HetCor data (Fig. 7a), we assign the ^{1}H peaks near 7.8 ppm primarily to the silanol protons. The silanol ^{1}H chemical shift indicates a moderate hydrogen bond of d(O···O) ≈ 2.8 Å according to the correlation of Yesinowski et al. (1988). The small width of the corresponding ^{2}H powder pattern for these environments (Fig. 4d) is also consistent with a moderate hydrogen bond interaction, with the measured C_q = 210 kHz corresponding to d(O···O) ≈ 2.76 Å, from the correlation of Poplett and Smith (1978).

Dehydrating the 10 Å phase to talc results in loss of the ^{1}H MAS peak at $\delta_{H\text{-}1}$ = 7.8 ppm (Fig. 3), leaving only two peaks that are coupled to Si, at $\delta_{H\text{-}1}$ = 3.8 and 0.8 ppm (Fig. 8). The HetCor data show that the peak at $\delta_{H\text{-}1}$ = 3.8 ppm is strongly coupled to the Q^2-type Si sites (Figs. 9 and 10) indicating that this peak arises from the silanol protons. This result indicates that a large change occurs in the chemical shift of the silanol protons upon removal of interlayer H_2O, from $\delta_{H\text{-}1}$ = 7.8 to 3.8 ppm, which is consistent with loss of the hydrogen-bond acceptor group—the interlayer H_2O. It is unlikely that the silanol H would be removed with dehydration of the 10 Å phase to talc. Studies of silica gel and zeolites (e.g., Bronnimann et al. 1988; Liu and Maciel 1996; Espinose de la Caillerie et al. 1997) have shown that isolated silanol groups give a ^{1}H chemical shift near 2.0 ppm, but that hydrogen bonding shifts the silanol peak position to more positive chemical shifts. For example, the ^{1}H spectrum of hydrated silica gel (Bronnimann et al. 1988) spans a broad range of chemical shifts, showing a peak maximum near +4 ppm and a tail toward more positive chemical shifts that overlaps the 7–8 ppm range, which corresponds to moderate hydrogen bonding interactions. The H_2O that is hydrogen bonded to silanols on the silica gel surface can be removed by exposure to vacuum (Liu and Maciel 1996), essentially converting hydrogen bonded silanols to isolated silanols. De-protonation of silanols can occur with heating, but is generally thought to require condensation of adjacent silanol groups to form a siloxane bridge plus H_2O molecule. Isolated silanols remain protonated to well over 500 °C in vacuum (Bronnimann et al. 1988). It is unlikely that such condensation reactions could occur easily upon dehydration of the 10 Å phase owing to the structural constraints that bonding to the octahedral sheet places on the 2:1 layer.

In all of the samples, the ^{1}H peak near 3.5 ppm represents the largest fraction of H after the Mg_3-OH sites, indicating assignment to interlayer molecular H_2O. This assignment is consistent with the corresponding component of the ^{2}H spectra (Fig. 4c), which appears to contain a characteristic signal for "flipping" H_2O molecules (e.g., Eckert et al. 1987) in addition to a contribution from more rigid water molecules. This chemical shift corresponds to H_2O molecules that are weak hydrogen bond donors; from the correlation of Yesinowski et al. (1988) this observed chemical shift suggests d(O···O) ≈ 2.98 Å. Compared to structural water molecules in other minerals, $\delta_{H\text{-}1}$ = 3.2 ppm for 10 Å phase S01 is most similar to those of analcime ($\delta_{H\text{-}1}$ = 3.1 ppm; Yesinowski et al. 1988), which do not participate in hydrogen bonds (Ferraris et al. 1972). The variation in the chemical shift for this peak among the samples (3.2–3.7 ppm; Table 1) reflects differences in the average hydrogen bond environment for interlayer H_2O.

The HetCor data for sample S01 show that the H of the interlayer H_2O are strongly coupled to the Q^2 and a subset of the Q^3 sites (Fig. 7b), indicating that they are closely associated with

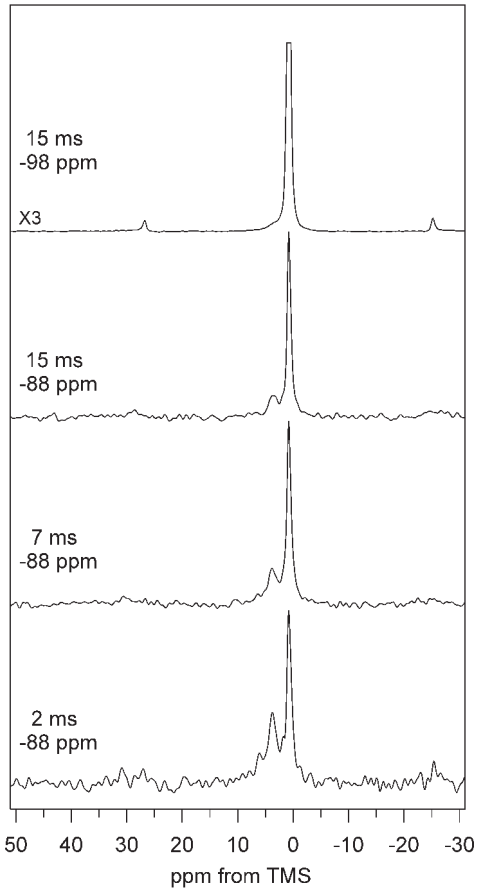

FIGURE 9. ^{1}H traces (*F*1) from ^{29}Si{^{1}H} HetCor spectra of S01d talc taken at the Q^2 peak position ($\delta_{Si\text{-}29}$ = –88 ppm) for the indicated contact times, and at a contact time of 15 ms for Q^3 at $\delta_{Si\text{-}29}$ = –98 ppm.

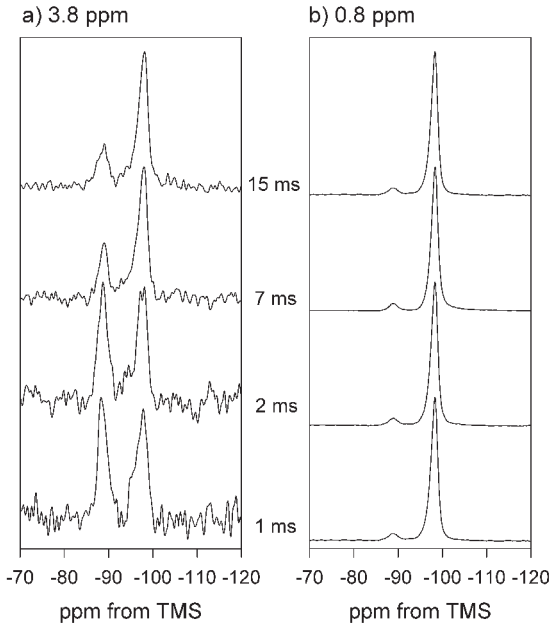

FIGURE 10. ^{29}Si traces (*F*2) from ^{29}Si{^{1}H} HetCor spectra of S01d talc taken at the indicated contact times. Traces correspond to the cross-sections at the main ^{1}H peak positions in *F*1 at (**a**) $\delta_{H\text{-}1}$ = 3.8, and (**b**) 0.8 ppm.

the vacancy defects in the 2:1 layers. In addition, the position of the Q^3 cross-peak is shifted by +1 ppm from that for the bulk Q^3 sites (–97 vs. –98 ppm), which might indicate some structural relaxation in these hydrated defects. The intensity ratio of the Q^2:Q^3 cross peaks at $\delta_{H\text{-}1}$ = 3.1 ppm is nearly constant (0.35:0.65) at contact times from 1 to 7 ms, which suggests that there is a subset of Q^3 that are strongly coupled to the H_2O protons. This cross-peak intensity ratio is very close to the 2:3 ratio for Q^2:Q^3 sites expected for a silicate ring that contains an isolated vacancy. The Q^3 cross-peak intensity increases at longer contact times owing to spin diffusion and possibly additional cross-relaxation to more distant Q^3 sites.

For sample S01, the relative intensity of the peak at 7.8 ppm in the ^{1}H MAS spectra is too large to be attributed solely to silanol protons based on mass balance considerations. Assuming that the vacancies in the tetrahedral sheets are isolated, as suggested by the results of Welch et al. (2006), then the vacancy concentration is one-third the concentration of Q^2 sites, which is about 10% of the Si. A structural formula for sample S01 can then be approximated as:

$$Mg_3(OH)_2Si_{3.49}(SiOH)_{0.38}(\square\text{-}HO)_{0.13}O_{9.49}{\cdot}xH_2O,$$

where (SiOH) are the silanol-terminated Q^2 sites and ($\square$-HO) represents the vacancy apical oxygens ($\square$-O-3Mg), which are assumed to be protonated for local charge balance. A distinct ^{1}H NMR signal that could be assigned to $\square$-HO sites was not observed, but the chemical shift for these ^{1}H is probably very similar to that for the bulk Mg_3-OH in the absence of significant hydrogen bonding interactions. The HetCor spectra did not show a significant change in the Q^2-detected Mg_3-OH chemical shift with contact time, consistent with the idea that the main hydroxyl peak includes signal from the $\square$-HO defect sites.

If the peak at $\delta_{H\text{-}1}$ = 0.9 ppm represents all the Mg_3-OH environments, then the expected ratio to silanol H is 5.6:1, significantly higher than the observed 3.6:1 intensity ratio for the peaks at 0.9 and 7.8 ppm in the ^{1}H MAS spectrum. Thus, we conclude that the peak at 7.8 ppm also includes signal from water molecules that donate moderate hydrogen bonds, corresponding to about one-third the intensity of this peak and about 10% of the total bound H_2O. This conclusion is supported by the much smaller intensity of the ~8 ppm signal in the summed HetCor projections (cf. Figs. 3a and 3b), which show only the rigid H in close proximity to Si. A fit of the HetCor projection obtained at 15 ms contact time (Fig. 3b) gives a ratio (0.63:0.11) equal to that expected from mass balance if the ^{29}Si-detected (HetCor) peak at 8 ppm arises only from silanol protons. This spectrum was obtained under conditions in which magnetization transfer was nearly equilibrated, with 93% of the fitted equilibrium Q^3 CP/MAS intensity ($T_{Si\text{-}H}$ = 5.6 ms; $T_{1\rho,H}$ >> 15 ms). Presence of some water molecules as hydrogen bond donors would also explain the slight difference in peak position between the Het-

Cor and MAS spectra (8.0 vs. 7.8 ppm). For the S01d talc, the intensity ratio for the ^{1}H MAS peaks assigned to Mg_3OH and silanols is also approximately 5:1 (Table 1), as expected for this proposed structural formula if the Q^2 concentration does not change with dehydration.

Assuming that the signal for the peak at $\delta_{H\text{-}1}$ = 7.8 ppm in excess of that expected for silanol H arises from H_2O molecules gives a value x = 1.2 for the NMR-detected structural H_2O content of the S01 sample. This value is consistent with thermogravimetric analyses for this sample (Evans and Guggenheim 1988, p. 256) and with the $x \approx 1.0$ value proposed in recent studies (Welch et al. 2006; Comodi et al. 2005). For a structure with phlogopite-like layer stacking, an interlayer H_2O content with $x > 1.0$ requires some 12-fold sites to contain more than one water molecule, which could result in hydrogen bond interactions between them. The H of the hydrogen bond donor could contribute to the signal intensity at $\delta_{H\text{-}1}$ = 7.8 ppm, which is very similar to the ^{1}H chemical shift of ice (Kinney et al. 1993).

The 10 Å phase samples prepared from talc at higher P and T appear to have significantly lower H_2O content, as indicated by the larger relative intensity of the main ^{1}H MAS peak for Mg_3-OH sites (Table 1). These samples also contain significantly less intensity for the peak near $\delta_{H\text{-}1}$ = 7.7 ppm, with intensity ratios to the main hydroxyl peak of between 4:1 and 6:1. Assuming that the peak near 7.7 ppm represents mostly silanol H, the fitted relative ^{1}H intensities for these samples (Table 1) suggest bound H_2O contents approximately $x \approx 0.8$ H_2O pfu (3 Mg), similar to that reported by Welch et al. (2006) for a sample prepared under similar conditions, but from oxide starting materials. Unfortunately, accurate Q^2 contents could not be obtained for these samples, so we cannot determine whether the peak near 7.8 ppm also contains H_2O as hydrogen bond donors. If these samples have Q^2 concentrations similar to those reported by Welch et al. (2006) for a sample prepared at similar P and T conditions but from brucite+silica starting materials (16%), then the signal at 7.8 ppm can be assigned solely to silanol groups. The 7.8 ppm SSB envelope in the ^{2}H NMR spectrum of HM-03 does not appear to contain a strong contribution from "flipping" H_2O molecules, but a small fraction cannot be ruled out based on this lineshape.

The differences observed in the ^{1}H NMR spectra for the 10 Å phase samples are striking and reflect variations in the structural relationship between interlayer H_2O and the 2:1 layers that also appears to change with time. For the samples prepared from talc (HM-0305 and HM-03) the decrease of chemical shift of the main hydroxyl peak from 1.6 to 1.2 ppm with storage time indicates a decrease in average hydrogen bond strength to interlayer H_2O. The peak position for sample S01 (>20 years old) is essentially the same as for talc, indicating no significant hydrogen bond interaction between the Mg_3-OH and interlayer H_2O. These observations are remarkably similar to the results of recent molecular dynamics (MD) studies of interlayer H_2O in talc by Wang et al. (2004, 2005). In simulations at pressure for the x = 2 composition, the Mg_3-OH serve as hydrogen bond donors to the interlayer H_2O molecules, but the water molecules do not interact strongly with other H_2O molecules. The difference in the chemical shift for the main hydroxyl peak between talc (0.9 ppm) and 10 Å phase shortly after synthesis (1.6 ppm for HM-0305) is consistent with the presence of a weak hydrogen bond. Upon decompression, Wang et al. (2005) report a 2-d ice-like structure forms among the H_2O molecules with reduced hydrogen bonding to the Mg_3-OH, which is consistent with our observation of a decreased chemical shift for the hydroxyl groups. The ^{1}H NMR data indicate that water molecules that donate ice-like hydrogen bonds could occur in sample S01, and perhaps also in the other samples. At lower pressure, the MD model suggests that the 2-d ice melts, giving some liquid-like H_2O sites, consistent with the relatively narrow peak near 4.0 ppm in the center band for HM-03 (Fig. 3c). In the simulations, these changes occur rapidly upon decompression, but the model does not include tetrahedral vacancies and silanol groups. These defect sites interact with the interlayer H_2O at 1 atm and could stabilize different interlayer H_2O structures. In addition, Wang et al. (2005) found a layer stacking for the x = 2 composition that differs from the mica-like stacking in models of the x = 1 composition (Wang et al. 2004) and observed by XRD ambient conditions (Comodi et al. 2005), which also suggest that several different structures are possible.

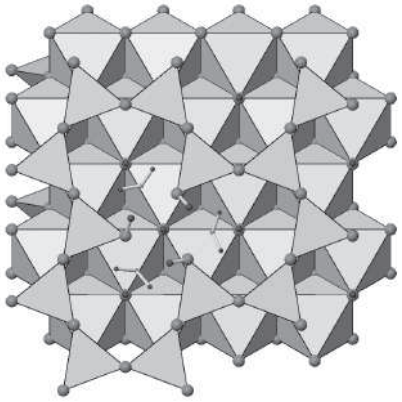

Figure 11. Polyhedral representation of a 2:1 layer of the 10 Å structure showing proposed isolated tetrahedral vacancy with three silanol groups hydrogen bonded to interlayer H_2O at d(O···O) = 2.8 Å (white dotted lines). Diagram constructed schematically by assuming ∠Si-O-H = 109.5° and ∠O-H…O = 180°; vacancy apical oxygen is shown protonated for local charge balance.

Structural implications for the 10 Å phase

Our results, considered with those of Welch et al. (2006), provide strong evidence that Si-vacancies and subsequent modification of the interlayer by silanol groups is an essential component of the 10 Å phase. Although the Q^2 fraction for sample S01 (10%) seems minor, this concentration corresponds to, on average, one silanol for each pair of 6-member silicate rings in the mica-like stacking. The Q^2 fractions reported by Welch et al. (2006) for other samples are even higher, corresponding to about one silanol per 6-member silicate ring. Thus, interaction with silanol groups likely affects a large fraction of the interlayer H_2O. For sample S01 about one-third of the interlayer water molecules accept a hydrogen bond from silanol groups.

Why do tetrahedral vacancies form with hydration of the interlayer? For pure talc, the siloxane planes are hydrophobic (e.g., Giese et al. 1991; Schrader and Yariv 1990), with no mechanism

for significant hydrogen bond interaction between the neutral bridging O atoms and an interlayer H_2O network (Wang et al. 2005). Introduction of silanol terminations at the Q^2 sites adjacent to Si-vacancies provides interlayer hydrogen bond donors that connect the interlayer $2H_2O$ and the talc host.

The NMR data show that the silanol groups in the 10 Å phase are much stronger hydrogen bond donors than the Mg_3-OH, with a moderate $d(O\cdots O) \approx 2.8$ Å obtained from both the ^1H and ^2H data. This hydrogen bond length is similar to that of the ice polymorphs (e.g., Jeffrey 1997, p. 143). At ambient conditions a common H_2O structure is an isolated water molecule hydrogen bonded to a silanol group, where the H of the water molecule do not serve as hydrogen bond donors (Fig. 11). However, these water molecules could interact with other interlayer H_2O molecules at elevated pressure and/or higher H_2O content. The inferred hydrogen bond strength for the 10 Å phase silanol groups [$d(O\cdots O) \approx 2.8$ Å] is weaker than the average for silanols in crystalline silicates reported by Nyfeler and Armbruster (1998), $d(O\cdots O) \approx 2.633$ Å, but similar to the few structures known in which the hydrogen bond acceptor is a water molecule (e.g., Ginderow 1988). Moderate hydrogen bonds usually exhibit nearly linear acceptor-H-donor geometry, which appears unlikely to be accommodated by the other oxygen atoms within or between siloxane planes. Considering that each of the silanol groups created by a vacancy can be directed toward the center of a different 6-membered silicate ring and tilted toward the interlayer space (e.g., Fig. 11), it seems this relatively short distance could easily be accommodated by a H_2O molecule.

The NMR data indicate that the 10 Å phase could contain several types of H_2O in the interlayer at ambient conditions, some of which accept moderate hydrogen bonds from silanol groups and others that are more weakly bound. Most of the interlayer H_2O appears to be very weak hydrogen bond donors, but we cannot rule out the presence of some hydrogen bonds between water molecules, especially at higher H_2O content. This distribution of hydrogen bond environments suggests that the interlayer H_2O probably exhibit positional disorder of the oxygen, in addition to the dynamical disorder involving the hydrogen atoms (e.g., Wang et al. 2004). Hydrogen bonding between a silanol group and water molecule should shift the oxygen atom of the H_2O away from the center of the 12-coordinated site formed by the basal O atoms of the pairs of 6-membered silicate rings (Fig. 11). However, the average oxygen position about a distribution of isolated tetrahedral vacancies would correspond to the center of the 12-coordinated sites, consistent with the position and large displacement parameters determined from XRD data (Comodi et al. 2005). The relatively small concentration of Si vacancies would be difficult to detect directly by X-ray diffraction methods.

The more strongly bound H_2O could contribute to the unusually large dehydration enthalpy for the 10 Å phase reported by Miller et al. (1991), 200 kJ/mol, which is significantly larger than that for tightly bound H_2O on hydrophilic oxide surfaces (120 kJ/mol; McHale et al. 1997). Furthermore, the differential thermal gravimetric (DTG) curve for the S01 sample clearly shows a second, smaller dehydration event near 550 °C (Evans and Guggenheim 1988) that might correspond to release of the H_2O that are hydrogen bonded to silanols.

We suggest that the H_2O-present formation of the 10 Å phase from talc occurs by a reaction with H_2O to form a Si-vacancy (□) terminated by hydroxyl groups plus silica, approximately:

$$H_2O + 3(\text{Si-O-Si}) + Mg_3\text{-O-Si} = 3(\text{Si-OH}) + Mg_3\text{-OH} + \square + SiO_2(s) \quad (1)$$

plus insertion of H_2O in the interlayer, the amount of which is probably variable. Evidence for a small amount of a hydrous silica-rich phase was noted by Welch et al. (2006) from $^{29}Si\{^1H\}$ CP/MAS spectra of a 10 Å phase sample prepared from stoichiometric talc, but the silica could remain dissolved in the presence of excess fluid at elevated *P*-*T*.

Assignments for vibrational bands and structural models for incorporation of H_2O in phyllosilicates at elevated *P* and *T* must be reconsidered for the 10 Å phase specifically, and perhaps for other phyllosilicates more generally, especially those with hydrophobic 2:1 layers. The silanol groups should yield distinct signals in infrared and Raman spectra and could explain some of the Raman bands that have been difficult to assign (Fumagalli et al. 2001). Structural variations in the interlayer H_2O structure and changes with storage time are clearly evident in our ^1H-NMR spectra of the 10 Å phase, in agreement with the molecular dynamics models of Wang et al. (2005). As a result, it appears that a full understanding of the interlayer H_2O structure, H_2O content, and interaction of the interlayer H_2O with the 2:1 layers must be carried out with in situ experimental methods. Furthermore, given the defect structure of the 10 Å phase, the chemical composition probably depends on *P* and *T*. Such complexity is suggested by the difference in Q^2 fraction for sample S01 compared to those studied by Welch et al. (2006), and the extra Q^2 peak observed in the spectrum of sample HM-03. Further work is needed to determine how the vacancy concentration depends on pressure and temperature. Comparison of spectroscopic data obtain at 1 atm (e.g., NMR vs. IR and Raman; Brunner et al. 1992), changes in vibrational spectra as functions of *P* and *T*, and comparison with computational models that include silanol terminations at tetrahedral vacancies should allow a greater understanding of the structure and stability of interlayer H_2O under mantle conditions.

Acknowledgments

We thank Mark Welch, Jim Kirkpatrick, and Andrey Kalinichev for helpful discussion, Donald Lindsley and Jennifer Kung for assistance with sample synthesis, and Martine Ziliox for help with the ^2H NMR experiments. H.M. was supported in part by the REU program in the Mineral Physics Institute at Stony Brook University (NSF EAR 0139436). Support was provided by the U.S. NSF under grants EAR-0310200 (B.L.P.) and EAR-0308588 (S.G.) and by the Petroleum Research Fund via grant PRF no. 43871-AC2 (S.G.).

References cited

Barron, P.F. and Frost, R.L. (1985) Solid state ^{29}Si NMR examination of the 2–1 ribbon magnesium silicates, sepiolite, and palygorskite. American Mineralogist, 70, 758–766.

Bauer, J.F. and Sclar, C.B. (1981) The "10 Å phase" in the system $MgO\text{-}SiO_2\text{-}H_2O$. American Mineralogist, 66, 576–585.

Bronnimann, C.E., Zeigler, R.C., and Maciel, G.E. (1988) Proton NMR study of dehydration of the silica gel surface. Journal of the American Chemical Society, 110, 2023–2026.

Brunner, E., Karge, H.G., and Pfeifer, H. (1992) On the correlation between the ^1H NMR chemical shift and the stretching vibration frequency of hydroxyl groups in solids. Zeitschrift für Physikalische Chemie, 176, 173–183.

Chinnery, N.J., Pawley, A.R., and Clark, S.M. (1999) In situ observation of the

formation of 10 Å phase from talc + H_2O at mantle pressures and temperatures. Science, 286, 940–942.
Comodi, P., Fumagalli, P., Nazzareni, S., and Zanazzi, P.F. (2005) The 10 Å phase: Crystal structure from single-crystal X-ray data. American Mineralogist, 90, 1012–1016.
Eckert, H., Yesinowski, J.P., Stolper, E.M., Stanton, T.R., and Holloway, J. (1987) The state of water rhyolitic glasses. A deuterium NMR study. Journal of Non-Crystalline Solids, 93, 93–114.
Espinose de la Caillerie, J.-B.d. and Fripiat, J.J. (1994) A reassessment of the ^{29}Si MAS-NMR spectra of sepiolite and aluminated sepiolite. Clay Minerals, 29, 313–318.
Espinose de la Caillerie, J.-B.d., Aimeur, M.R., El Kortobi, Y., and Legrand, A.P. (1997) Water adsorption on pyrogenic silica followed by ^{1}H MAS NMR. Journal of Colloid and Interface Science, 194, 434–439.
Evans, B.W. and Guggenheim, S. (1988) Talc, pyrophyllite and related minerals. In S.W. Bailey, Ed., Hydrous Phyllosilicates (Exclusive of Micas), 19, p. 225–294. Reviews in Mineralogy, Mineralogical Society of America, Chantilly, Virginia.
Ferraris, G., Yerkess, J., and Jones, D.W. (1972) Neutron diffraction study of the crystal structure of analcime, $NaAlSi_2O_6 \cdot H_2O$. Zeitschrift für Kristallographie, 135, 240–252.
Fumagalli, P. and Poli, S. (2005) Experimentally determined phase relations in hydrous peridotites to 6.5 GPa and their consequences on the dynamics of subduction zones. Journal of Petrology, 46, 555–578.
Fumagalli, P., Stixrude, L., Poli, S., and Snyder, D. (2001) The 10 Å phase: a high-pressure expandable sheet silicate stable during subduction of hydrated lithosphere. Earth and Planetary Science Letters, 186, 125–141.
Fyfe, C.A., Zhang, Y., and Aroca, P. (1992) An alternative preparation of organo-functionalized silica gels and their characterization by two-dimensional high-resolution solid-state heteronuclear NMR correlation spectroscopy. Journal of the American Chemical Society, 114, 3252–3255.
Giese, R.F., Costanzo, P.M., and Vanoss, C.J. (1991) The surface free energies of talc and pyrophyllite. Physics and Chemistry of Minerals, 17, 611–616.
Ginderow, D. (1988) Structure l'uranophane alpha, $Ca(UO_2)_2(SiO_3OH)_2 \cdot 5H_2O$. Acta Crystallographica, C44, 421–424.
Jeffrey, G.A. (1997) An Introduction to Hydrogen Bonding, 303 p. Oxford University Press, New York.
Johnson, M.C. and Walker, D. (1993) Brucite [$Mg(OH)_2$] dehydration and the molar volume of H_2O to 15 GPa. American Mineralogist, 78, 271–284.
Khisina, N.R. and Wirth, R. (2002) Hydrous olivine ($Mg_{1-y}Fe^{2+}_y)_{2-x}v_xSiO_4H_{2x}$—a new DHMS phase of variable composition observed as nanometer-sized precipitations in mantle olivine. Physics and Chemistry of Minerals, 29, 98–111.
Kinney, D.R., Chuang, I.S., and Maciel, G.E. (1993) Water and the silica surface as studied by variable-temperature high-resolution ^{1}H NMR. Journal of the American Chemical Society, 115, 6786–6794.
Koch-Müller, M., Matsyuk, S.S., Rhede, D., Wirth, R., and Khisina, N. (2006) Hydroxyl in mantle olivine xenocrysts from the Udachnaya kimberlite pipe. Physics and Chemistry of Minerals, 33, 276–287.
Kolodziejski, W. and Klinowski, J. (2002) Kinetics of cross-polarization in solid-state NMR: A guide for chemists. Chemical Reviews, 102, 613–628.
Liu, C.H. and Maciel, G.E. (1996) The fumed silica surface: A study by NMR. Journal of the American Chemical Society, 118, 5103–5119.
Mägi, M., Lippmaa, E., Samoson, A., Engelhardt, G., and Grimmer, A.R. (1984) Solid-state high-resolution silicon-29 chemical shifts in silicates. Journal of Physical Chemistry, 88, 1518–1522.
McHale, J.M., Navrotsky, A., and Perrotta, A.J. (1997) Effects of increased surface area and chemisorbed H_2O on the relative stability of nanocrystalline γ-Al_2O_3 and α-Al_2O_3. Journal of Physical Chemistry B, 101, 603–613.
Miller, A.K., Guggenheim, S., and Koster van Groos, A.F. (1991) The incorporation of "water" in a high-pressure 2–1 layer silicate: A high pressure differential thermal analysis of the 10 Å phase. American Mineralogist, 76, 106–112.
Nyfeler, D. and Armbruster, T. (1998) Silanol groups in minerals and inorganic compounds. American Mineralogist, 83, 119–125.
Oglesby, J.V. and Stebbins, J.F. (2000) ^{29}Si CPMAS NMR investigations of silanol-group minerals and hydrous aluminosilicate glasses. American Mineralogist, 85, 722–731.
Pawley, A.R. and Wood, B.J. (1995) The high-pressure stability of talc and 10 Å phase: potential storage sites for H_2O in subduction zones. American Mineralogist, 80, 998–1003.
Perrillat, J.P., Daniel, I., Koga, K.T., Reynard, B., Cardon, H., and Crichton, W.A. (2005) Kinetics of antigorite dehydration: A real-time X-ray diffraction study. Earth and Planetary Science Letters, 236, 899–913.
Poplett, I.J.F. and Smith, J.A.S. (1978) Deuteron quadrupole resonance studies 8. ^{1}H-^{2}H double resonance in some inorganic hydroxy compounds. Journal of the Chemical Society—Faraday Transactions, 74, 1077–1087.
Rocha, J., Welch, M.D., and Klinowski, J. (1991) ^{29}Si Magic-Angle-Spinning NMR spectroscopy quantitatively monitors the double-chain/triple-chain intergrowths in hydrous silicates. Journal of the American Chemical Society, 113, 7100–7103.
Schrader, M.E. and Yariv, S. (1990) Wettability of clay minerals. Journal of Colloid and Interface Science, 136, 85–94.
Sclar, C.B., Benimoff, A.I., and Begley, A.L. (1987) Regular interstratification of brucite and the 10 Å phase, a high pressure phyllosilicate in the system MgO-SiO_2-H_2O. EOS Transactions of the American Geophysical Union, 68, 433.
Wang, J.W., Kalinichev, A.G., and Kirkpatrick, R.J. (2004) Molecular modeling of the 10 Å phase at subduction zone conditions. Earth and Planetary Science Letters, 222, 517–527.
——— (2005) Structure and decompression melting of a novel, high-pressure nanoconfined 2-D ice. Journal of Physical Chemistry B, 109, 14308–14313.
Weiss, C.A., Altaner, S.P., and Kirkpatrick, R.J. (1987) High-resolution ^{29}Si NMR spectroscopy of 2–1 layer silicates: correlations among chemical shift, structural distortions, and chemical variations. American Mineralogist, 72, 935–942.
Welch, M.D., Pawley, A.R., Ashbrook, S.E., Mason, H.E., and Phillips, B.L. (2006) Si vacancies in the 10 Å phase. American Mineralogist, 91, 1707–1710.
Wunder, B. and Schreyer, W. (1992) Metastability of the 10 Å phase in the system MgO-SiO_2-H_2O (MSH). What about hydrous MSH phases in subduction zones? Journal of Petrology, 33, 877–889.
Yamamoto, K. and Akimoto, S.I. (1977) System MgO-SiO_2-H_2O at high pressures and temperatures: stability field and hydroxyl chondrodite, hydroxyl clinohumite and 10 Å-phase. American Journal of Science, 277, 288–312.
Yesinowski, J.P. and Eckert, H. (1987) Hydrogen environments in calcium phosphates: ^{1}H MAS NMR at high spinning speeds. Journal of the American Chemical Society, 109, 6274–6282.
Yesinowski, J.P., Eckert, H., and Rossman, G.R. (1988) Characterization of hydrous species in minerals by high-speed ^{1}H MAS-NMR. Journal of the American Chemical Society, 110, 1367–1375.
Zumbulyadis, N. (1986) Hydrogen-silicon nuclear spin correlations in α-Si:H: a two-dimensional NMR study. Physical Review B, 33, 6495–6496.

MANUSCRIPT RECEIVED AUGUST 13, 2006
MANUSCRIPT ACCEPTED MARCH 21, 2007
MANUSCRIPT HANDLED BY MICHAEL FECHTELKORD